Mine Water and the Environment (2022) 41:176–193
https://doi.org/10.1007/s10230-021-00832-9

TECHNICAL ARTICLE

Determination of Evaporation from a Tailings Storage Facility Using Field Measurements and Satellite Observations

David McJannet[1] · Geoff Carlin[1] · Catherine Ticehurst[2] · Anna Greve[3] · Carolina Sardella[3]

Received: 16 February 2021 / Accepted: 11 September 2021 / Published online: 23 September 2021

Abstract

Most mining operations produce waste material, or tailings, which is commonly stored within impoundments known as tailings storage facilities (TSFs). A common TSF design involves depositing slurry on tailings 'beaches' which are sloped towards a containing wall or central pond which collects excess water. A crucial aspect of safely operating TSFs is managing the residual moisture content of the deposited tailings, which requires an accurate understanding of the water balance of the TSF. However, evaporation from a TSF is particularly hard to quantify as the degree of surface wetness varies spatially and temporally, and moisture content depends on the time since tailings deposition and the prevailing climate. This study addresses these issues at an active TSF by combining field measurements, models, and satellite observations. Evaporation from open water was measured using a floating evaporation pan and evaporation from the tailings beaches was investigated using micro-lysimeter measurements. Evaporation rates for different moisture contents were expressed as a fraction of open water evaporation and a strong relationship was developed for use in satellite analysis. Spatial and temporal patterns of open water and moisture content were determined at 20 m resolution using moisture indices applied to Sentinel-2 satellite scenes. Continuous open water evaporation rates and spatial moisture content information were combined to estimate total TSF evaporation. Comparison of TSF evaporation rates to those derived using an existing site water balance model showed very good agreement. The methodology developed could be applied at other locations around the world.

Keywords Tailings beaches · TSF · Open water · Sentinel-2

Introduction

Globally, it is estimated that between five to fourteen billion tonnes of tailings are produced from mining activities each year (Jones and Boger 2012; Schoenberger 2016). This material needs to be safely stored for future processing and treatment. Storage of this material is approached in a number of ways depending on mine site characteristics and the composition of the waste material, but one of the most widely used approaches is to build surface tailings storage impoundments (Adiansyah et al. 2015; Edraki et al. 2014). Tailings can be delivered to these impoundments in a variety of ways, but the most common form is as a slurry. These tailings storage facilities (TSFs) aim to spread the waste material in thin layers to aid with dewatering and consolidation through evaporation and drainage. A common TSF design involves depositing slurry on tailings 'beaches' that are sloped towards a containing wall or central decant pond which collects the supernatant water for reprocessing.

Safe operation of TSFs relies on geotechnically stable tailings, which is directly related to the residual moisture content of the stored material. Managing the residual moisture content of tailings requires an accurate understanding of the inflows and outflows of solids and water and of how changes to deposition practice will affect these flows. The main flows of water include pumped inflows and outflows and evaporation. While pumped flows into and out of TSFs are typically well known, evaporation losses are not as well understood. A TSF presents a challenge to evaporation estimation because at any point in time, the surface of the TSF can be characterised by either open water (i.e. decant pond) or tailings beaches of varying degrees of wetness.

✉ David McJannet
david.mcjannet@csiro.au

[1] CSIRO, EcoSciences Precinct, GPO Box 2583, Dutton Park, QLD 4001, Australia

[2] CSIRO, Black Mountain, ACT, Australia

[3] McArthur River Mine, Glencore, NT, Australia

The degree of wetness varies spatially over time and local moisture content typically depends on the time since local deposition and the prevailing climate.

Evaporation has long been recognised as one of the more difficult water balance components to accurately specify for a TSF. It is common for a TSF water balance to be established using an approach where evaporation is crudely represented as some fraction of potential or class A pan evaporation (e.g. Leavy 2018; Solgi 2017) or using numerical models (e.g. Rykaart et al. 2001; Šimůnek et al. 2008) that estimate evaporation using the hydraulic properties of tailings. Such approaches have a high degree of uncertainty, which has led others to investigate TSF evaporation using laboratory and field studies.

Some studies have taken tailings material into the lab and monitored evaporation from columns and pans under controlled energy input and wind conditions. The study findings have then been used to parameterise evaporation models for use at specific sites (e.g. Fisseha et al. 2010; Simms et al. 2007). Other field studies have measured evaporation rates using micro-lysimeters and micro-meteorological techniques (e.g. Fujiyasu et al. 2000; Newson and Fahey 2003), but these have focused on materials that are drying over extended periods rather than continually cycling through wetting and drying regimes.

The two key components missing from most of the previous studies are: (1) the ability to explicitly account for spatial and temporal variation in tailings beach moisture content, and (2) the ability to define the varying spatial extent and location of the decant pond. The aim of this current study was to address these issues by using an approach that combined field measurements and satellite observations. The field measurements were intended to produce a relationship between the evaporation rate and surface moisture content, while the satellite analysis provided the temporal and spatial variability in surface moisture content and decant pond extent. An active TSF at McArthur River Mine was selected for technique development.

Study Site

The McArthur River Mine (MRM) is a zinc and lead mine situated on the McArthur River, about 970 km southeast of Darwin, Australia (− 16.4208°, 136.1082°). The TSF covers an area of around 130 ha (Fig. 1) and is a beach deposition style operation where tailings slurry is released from spigot points located around the outside edge of the TSF. The tailings are deposited on the beaches and the water drains to the central decant pond from which it is pumped back out of the system. Spigots are typically activated in sets of three with rotation controlled by the head of TSF operations in response to the evolution of the tailings beach surface. At any point in time, the surface of the TSF can be characterized by either open water or tailings of varying degrees of drying.

Materials and Methods

Open Water Evaporation

Floating Evaporation Pan

Evaporation from the open water section (i.e. decant pond) of the TSF was measured over a 72-day period using a floating evaporation pan. The design of the floating evaporation pan used in this study builds on that used in previous studies (McJannet et al. 2019; McJannet et al. 2017) and is shown

Fig. 1 Drone imagery showing the layout of the McArthur River Mine TSF. The yellow points are the locations of spigots which are activated to release tailings onto the TSF. Water drains to the middle of the TSF. The red dot indicates the location of the floating evaporation pan and the blue dot indicates the locations of the land-based monitoring station (details in Sect. 2). The inset map shows the location of McArthur River Mine in Australia

in Fig. 2. The evaporation pan had the same dimensions as a standard Class-A evaporation pan (1207 mm diameter and 254 mm deep) and was supported by a floating frame that also provided mounting points for sensors and data loggers. When filled with water, the pan was entirely immersed apart from the top 70 mm; this helped the pan maintain thermal equilibrium with the surrounding water. The frame was contained within a larger PVC pipe structure designed to deflect wave energy away from the pan, thereby increasing data quality and retention rates. The floating pan rotated around its anchoring point in response to prevailing winds.

Operation of the evaporation pan was fully automated with any evaporated water being replenished each 24 h period by pumping. Water level in the pan was measured using a high accuracy and precision magnetostrictive linear-positioning sensor (GH-Series, MTS Sensors, USA), which was installed within a stilling well in the pan. The full measurement range of the sensor was 150 mm, resulting in a linearity deviation of just 0.05 mm and a repeatability of 0.03 mm.

Supplementary measurements of wind speed, wind direction, air temperature, and humidity were made at a height of 1.0 m (WXT536, Vaisala, Helsinki, Finland). To ensure that conditions within the pan did not deviate too greatly from those in the decant pond, sensors were installed to measure the lake and pan skin temperature (SP-411, Apogee Instruments, Utah, USA). All sensors were measured at 15 s intervals with average, total, maximum, and minimum values recorded at 30 min intervals.

Evaporation from the pan was determined on a daily timestep using the difference in water level measured in the pan from the time of last refilling. Despite the best efforts to maintain thermal equilibrium between water within the pan and water in the surrounding lake through immersion of the pan and regular water replenishment, some deviation in temperature will be inevitable due to heat storage differences. Evaporation from the pan was corrected for any effects of water temperature difference between the water in the pan and the surrounding water body using the correction procedure proposed by McJannet et al. (2017). Using this approach open water evaporation, E_{ow} (mm day^{-1}), was calculated as;

$$E_{ow} = E_{pan} \frac{\left(e^*_{ow} - e_{air}\right)}{\left(e^*_{pan} - e_{air}\right)} \quad (1)$$

where E_{pan} (mm day^{-1}) is the evaporation from the immersed pan, e^*_{ow} (kPa) is the saturated vapour pressure at the water surface temperature of the open water, e^*_{pan} (kPa) is the saturated vapour pressure at the water surface temperature of the floating pan and e_{air} (kPa) is the vapour pressure of the air. This scaling approach was applied at 30 min intervals based on average values over that period. This assumes that the meteorological conditions experienced at the pan and by the surrounding lake are the same and that the differences in evaporation are related only to differences in the surface temperature of the two evaporating surfaces.

The final evaporation dataset included only the highest quality data. Data periods were excluded when wind or waves caused water to splash into or out of the pan, when rainfall occurred, when the pan was being remotely flushed or when equipment was being serviced. Problematic wind and wave action conditions were identified by obvious additions of water to the pan during the day and increased ranges (> 2 mm) in maximum and minimum depth measurements within the stilling well in the pan (McJannet et al. 2017).

Fig. 2 Floating evaporation pan deployed on the open water area of the TSF

Land Based Monitoring Station

To complement the evaporation measurements, a land-based monitoring station was also installed on the TSF wall (location shown in Fig. 1). This monitoring station was operational for the entire study, which commenced on 10 Aug. 2019 and ran until 15 Feb. 2020 (190 days). The main purpose of this station was to provide a means by which to predict evaporation on any given day using a range of measured climate variables. The methodology to achieve this involved using concurrent measurements from the land-based station and the evaporation system to develop a model for predicting open water evaporation (see further discussion below).

The land-based station was fitted with sensors for measuring solar radiation (CS320, Campbell Scientific, Utah, USA), wind speed and direction (RMY 03002, RM Young, Michigan, USA), air temperature and humidity (CS215, Campbell Scientific, Utah, USA), and rainfall (TB3, HyQuest Solutions, Sydney, Australia). In addition, the station had an extended horizontal arm that was fitted with sensors for measuring the surface temperature (SP-411, Apogee Instruments, Utah, USA) of the open water of the TSF.

All sensors were measured at 15 s intervals with average, total, maximum, and minimum values recorded at 30 min intervals.

Open Water Evaporation Modelling

Modelling of evaporation from the open water section of the TSF (E_{ow}, mm day^{-1}) was achieved using mass-transfer modelling approaches (Dalton 1802), which take the following form:

$$E_{ow} = f(U_L)(e^*_{ow} - e_{air}) \quad (2)$$

where $f(U_L)$, is a wind function (mm day^{-1} kPa^{-1}) which describes the diffusion mechanism by which thermal energy is removed from the surface as vapour. For the modelling in this investigation, the wind function was based around wind speed measurements at the land-based monitoring station (U_L). The wind function, $f(U_L)$, is unique to each open water environment and was derived using concurrent evaporation and meteorological observations. The linear form of the wind function (Weilenmann 1877) was given by:

$$f(U_L) = (a + bU_L) \quad (3)$$

where the terms a and b were derived by plotting measured daily average wind speed against $E_{ow}/(e^*_{ow} - e_{air})$. Once the wind function was defined, evaporation was subsequently calculated using Eq. (2) with the meteorological measurements from the land-based monitoring station.

Tailings Beach Evaporation

Micro-Lysimeter Study

Evaporation from tailings with different moisture characteristics was determined using the micro-lysimeter approach. Micro-lysimeters are small cores of intact soil contained within a section of PVC pipe that can be weighed at 24 h intervals to determine loss of water due to evaporation (Boast and Robertson 1982; McJannet et al. 2000).

The micro-lysimeters used in this study were constructed from 150 mm lengths of 90 mm diameter PVC pipe. Tailings cores were obtained by pushing the micro-lysimeters into the tailings and then excavating around them to enable the undisturbed core and PVC pipe section to be removed. The bottom end of the micro-lysimeter was capped with aluminium foil, which was held in place with electrical tape. The foil facilitates vertical heat transfer and keeps the soil core contained. While the capping may impede vertical movement of water, the short duration of observations, the absence of a shallow subsurface water table, and the core length used, all helped to minimise such effects on evaporation.

Each micro-lysimeter had a matching sleeve, which was constructed from slightly larger 100 mm diameter PVC pipe. These sleeves were pushed into the tailings beach at the selected measurement location and the tailings within were carefully excavated to enable the micro-lysimeter to be installed flush with the beach surface. Micro-lysimeters were weighed prior to installation using portable field scales (Scout SKX6201, Ohaus) with a precision of 0.1 g. The micro-lysimeters were removed from their sleeves at 24 h intervals and reweighed. This process was repeated for five 24 h periods commencing on 12 Aug. 2019. The weight difference in grams was converted to evaporation loss in mm based on the surface area of the micro-lysimeters.

Different authors have reported different lengths of time over which micro-lysimeters provide reliable measurements (e.g. Evett et al. (1995) – 9 days, Boast (1986) – 4 to 10 days, Daamen et al. (1993) – 7 days), and our 5 day observation periods falls safely within these limits. At the end of the 5 days, the tailings from each micro-lysimeter were dried in the oven at 105 °C for 48 h to determine the final gravimetric water content. Tailings water content at the start of each of the five days of observation was backcalculated by adding the weight of evaporated water for each measurement day to the end weight. Using this method, the evaporation rate relative to moisture content on a given day was derived. The moisture content was important as the aim was to express the evaporation rate as a fraction of a completely saturated surface (i.e. open water). Open water evaporation from the floating evaporation pan was considered a reference point for each day of observations. Gravimetric moisture content was used in the micro-lysimeter study (and sampling described below) rather than volumetric values for consistency with units used by other site operations dealing with tailings management, and for easier and safer collection and processing of samples.

The micro-lysimeters were filled with tailings covering a range of gravimetric moisture contents from slurry (≈0.7 g g^{-1}) to consolidated tailings (0.17 g g^{-1}). Slurry samples were put in micro-lysimeters with PVC caps glued on the end to prevent leakage. Three replicates of tailings representing dry, intermediate, wet, and recently deposited slurry (i.e. 12 micro-lysimeters in total) were placed in the micro-lysimeters and each was measured for five consecutive days. Variability in moisture content for micro-lysimeter sample selection was determined qualitatively by visual inspection. Micro-lysimeter measures took place over just one five-day measurement period during the study due to safety concerns for staff working on and around the TSF. The aim of the micro-lysimeter study was to produce a relationship between the moisture content of the TSF surface and evaporation for that day, expressed as a fraction of open water evaporation.

TSF Evaporation

Tailings Moisture Content from Satellite

Satellite imagery was used to derive the spatial pattern of moisture content across the TSF. The frequent revisit period and a high spatial resolution of the European Space Agency's Sentinel-2 A and -2B satellites made them ideal candidates for the task. Both satellites provide coverage of the TSF area, providing an overpass interval of 5 days. The Sentinel-2 satellite products are restricted by cloud-cover, but this is in part compensated for by the more frequent overpass interval. The Sentinel-2 satellites provide multispectral data with 13 bands in the visible, near-infrared, and short-wave infrared parts of the spectrum. The first task in satellite scene processing was to define a relationship between tailings moisture content and the spectral information captured by Sentinel-2.

Of particular interest to this study was the normalised difference moisture index (*NDMI*), which has been shown to represent spatial variations in vegetation and surface moisture (Mallick et al. 2012; Wilson and Sader 2002). The amount of water available near the surface largely controls the spectral reflectance in the shortwave infrared (*SWIR*) interval of the electromagnetic spectrum. *SWIR* reflectance is negatively related to water content. The *NDMI* is given by the ratio of the difference and the sum of the reflected radiation in the near infrared (*NIR*) and *SWIR*;

$$NDMI = \frac{(NIR - SWIR)}{(NIR + SWIR)} \quad (4)$$

For Sentinel-2, band 8 (central wavelength 842 nm) and 11 (central wavelength 1610 nm) were used for NIR and SWIR respectively. As the TSF is completely free from vegetation changes, the *NDMI* mainly reflects changes in surface moisture content. Using Sentinel-2 scenes, the *NDMI* was calculated at a spatial resolution of 20 m.

To define the relationship between *NDMI* and surface moisture content, Sentinel-2 satellite images were sourced for all overpass dates between January 2019 and February 2020. Atmospherically corrected Sentinel-2 scenes (level 2 A) are provided with scene classification level (SCL) information, which includes cloud probability classification information; this was used to exclude scenes with more than a medium probability of clouds (SCL ≥ 8). The remaining cloud-free scenes were extracted from the Digital Earth Australia data cube as NBAR-corrected surface reflectance (Geoscience Australia 2020, Digital Earth Australia, Sentinel-2. https://docs.dea.ga.gov.au/notebooks/DEA_datasets/Sentinel_2.html, viewed 13 March 2020). NBAR is the Nadir-Corrected BRDF (bidirectional reflectance distribution function) adjusted reflectance, meaning that the images are corrected for angular variation in reflectance. Further processing was then undertaken to limit analysis to only the tailings beach area of the TSF. This was achieved by applying a mask to the data to exclude non-TSF areas (i.e. roads and embankments) and areas of the TSF that could be inundated by water (i.e. decant) during the study period.

Initial inspection of the *NDMI* revealed that the index was unreliable in areas where salt had accumulated on the tailings surface as the tailings dried; therefore, the next step was to exclude salt-affected areas from further analysis. Salt-affected areas were identified in Sentinel-2 images using the visible bands. Following a trial and error approach alongside matching true colour Sentinel images, a pixel was deemed to be salt affected if the red band reflectance value > 0.15, the green band reflectance > 0.15, and the blue band reflectance was > 0.1. Pixels identified as being salt affected were excluded from further analysis.

Following this pre-processing, the *NDMI* value for every TSF beach pixel in every available scene was then compiled and the frequency distribution was calculated. The frequency distribution analysis counts how often values fall within a given range of *NDMI* in the entire dataset. The 1st and 99th percentile *NDMI* values were calculated to exclude outliers, and these were set as the maximum and minimum observed values for the TSF beaches.

Ideally, conversion of *NDMI* to tailings moisture content would involve collection of spatially distributed tailings samples across the full range of moisture content experienced across the TSF and comparison of these moisture contents to the corresponding *NDMI* to derive a calibration equation. However, extensive spatial sampling was not permitted due to safety concerns. Some limited spatial sampling (n = 67) was undertaken in drier areas on 12 Aug. 2019 and further samples (n = 56) were collected from the edge of the TSF on 11 Oct. 2019; this data was used to develop calibration relationships. During these two sampling campaigns, a 5 cm diameter push tube was used to extract 5 cm deep cores of tailings material, which were bagged and labelled for lab analysis.

Given the sampling constraints, the approach adopted involved relating maximum and minimum *NDMI* values to the maximum and minimum observed gravimetric moisture contents using a linear regression model. A simple linear fit between the two extremes is supported by similar soil moisture analysis undertaken in other studies using the *NDMI* (Gao 1996; Jovanovic et al. 2014; Xu et al. 2020). Justification for the linear fit to the *NDMI* vs. moisture content relationship will be further explored in the discussion section below. The points representing minimum and maximum tailings moisture content for the TSF were derived using samples from the micro-lysimeter study and occasional sampling around the TSF. Once the relationship

between *NDMI* and moisture content was defined, processing of Sentinel-2 scenes for full TSF spatial evaporation estimates could be undertaken.

Spatial Evaporation Prediction

To determine TSF evaporation across the study period, cloud-free Sentinel-2 scenes were sourced for the period between 10 Aug. 2019 and 15 Feb. 2020. Next, the extent of open water in each scene was identified using the modified normalised difference water index (*mNDWI*) proposed by Xu (2006);

$$mNDWI = \frac{(Green - SWIR)}{(Green + SWIR)} \quad (5)$$

The *mNDWI* was calculated using the shortwave infrared band (*SWIR*) and the green band (*Green*), which for Sentinel-2 are bands 11 and 3, respectively. An *mNDMI* value > 0.2 was used to define open water extent. This value was derived from a comparison of surface water extent in a drone image and a Sentinel-2 image from the same date.

As discussed earlier, salt accumulation prevented reliable application of the *NDMI*. Addressing this issue required a two-step process of identifying salt-affected areas and then assigning a suitable moisture content. These areas were identified using the same methodology described above.

Assigning a gravimetric moisture content to salt-affected areas was more complicated as tailings sample collection was restricted due to health and safety concerns. Two successful, but restricted, sample collection campaigns were undertaken, the first was on 12 Aug. 2019 and the second was on 11 Oct. 2019. During the first campaign, samples were taken from areas that could be safely accessed on foot, with these locations being mainly restricted to the dry areas that tended to have a salt build-up on the surface. During the second campaign, sampling was restricted to the edge of the TSF and again, most of these samples represented salt-affected areas. The moisture content derived during these two campaigns was used to derive a representative moisture content for salt-affected areas, which was applied across all scenes.

The moisture content of the remaining areas of the TSF were determined by calculating the *NDMI* and subsequently determining tailings moisture content using the methods described above. The moisture content of each pixel was then used to determine its evaporation rate as a fraction of open water evaporation and, subsequently, the modelled open water evaporation rate for the date of the satellite scene was used to calculate the spatially distributed evaporation rate and total evaporation for each 20 × 20 m pixel for a given day.

Daily TSF Evaporation

Using the methodology above, evaporation from the TSF was estimated for each day that clear Sentinel-2 scenes were collected. These satellites had a return period of 5 days and were occasionally affected by clouds which meant that a method was required to estimate evaporation for the days between usable satellite scenes. Infilling was achieved using daily open water evaporation estimates made throughout the study period. The total TSF evaporation for the days surrounding the periods to be infilled were first expressed as a ratio of observed evaporation ($\sum E_{TSF}$ expressed in ML) to total TSF evaporation assuming the entire TSF was open water ($\sum E_O$ also expressed in ML). The evaporation ratio for the day prior to the period to be infilled and the day after the period to be infilled were then averaged and this average value was then multiplied by the total possible open water evaporation (i.e. daily $\sum E_O$) for each day between satellite overpasses to estimate daily TSF evaporation.

Existing Water Balance Method

The estimates of TSF evaporation derived in this study were also compared to the operational method historically used for water balance analysis at MRM. The operational approach uses a site-wide water balance model (GoldSim™) in which the TSF is a dynamic water storage. The water balance model tracks water movement within the TSF over time based on inputs (e.g. rainfall, surface runoff, pumped water inflows, pumped tailings slurry inflows), outputs (e.g. evaporation, seepage, storage overflows, pumped outflows, entrained in situ moisture), change in stored water and solids inventory and specified operating rules.

A full description of the modelling approach is given in MRM (2017). For the purposes of this study, the total TSF evaporation rate was compared for the 157-day period between 10 Aug. 2019 and 13 Jan. 2020. While site water balance modelling continued past this date, a new TSF storage was added to the model and the two storages cannot be separated for individual analysis.

Results

Open Water Evaporation

Using a 6-day period in November 2019 as an example, Fig. 3 shows some typical traces of water level measured within the pan. The traces show the average, minimum, and maximum water level recorded in each 30 min period with the range being used as a guide to the level of wave action within the pans and the reliability of measurements. Shaded in grey are periods removed from analysis due to rainfall

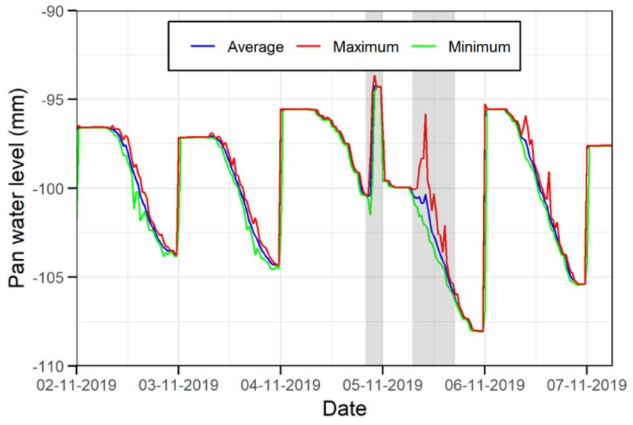

Fig. 3 Water level traces from evaporation pan for demonstration period. Periods excluded for poor data are indicated by grey shading

and excessive wave action. A combination of level sensor observations, rainfall observations, and servicing schedules were used to eliminate periods of unreliable data through the entire data set. Floating evaporation pan measurements were made over a 72 day period. Evaporation was analyzed over 12-h periods from midnight to midday and midday to midnight. After excluding poor-quality data, a total of 116 12-h evaporation periods were available for open water model development.

The high-quality measurement data for the first 72 days of observations are shown in Fig. 4. A linear regression has been fit to this data to derive a site-specific wind function, $f(U_L)$. Derivation of the wind function showed a strong relationship ($R^2 = 0.83$) between wind speed and $E_{ow}/(e^*_{ow} - e_{air})$. The site-specific wind function was used in the mass-transfer evaporation model (Eq. 2) to provide evaporation estimates:

$$E_{ow} = (1.23 + 1.36U_L)(e^*_{ow} - e_{air}) \quad (6)$$

The evaporation model (6) was applied to all 190 days of data from the land-based monitoring station to produce a complete record of daily open water evaporation rate (E_{ow}, mm day^{-1}) for the entire study period (Fig. 5). The average rate of evaporation was 7.0 mm day^{-1}. The complete dataset ignores the fact that there was a period between 19 Dec. 2019 and 20 Jan. 2019 when the TSF did not have an open water surface because the system had run dry. Open water evaporation was calculated for these days since evaporation rates across the TSF continued to be expressed as a fraction of open water evaporation. Calculating evaporation on days with no open water in the TSF created an additional problem since water surface temperature is used in the evaporation model and there was no water surface to measure. To overcome this problem, analysis was undertaken to derive a relationship between $(e^*_{ow} - e_{air})$ and $(e^*_{air} - e_{air})$ for days when open water was present. A very strong linear relationship was derived ($R^2 = 0.90$) and this was used to approximate $(e^*_{ow} - e_{air})$ data for days without water surface observations:

$$(e^*_{ow} - e_{air}) = 0.54(e^*_{air} - e_{air}) + 0.34 \quad (7)$$

The volume of water lost from each Sentinel-2 pixel identified as open water was determined by multiplying the evaporation rate by the pixel area (20 × 20 m).

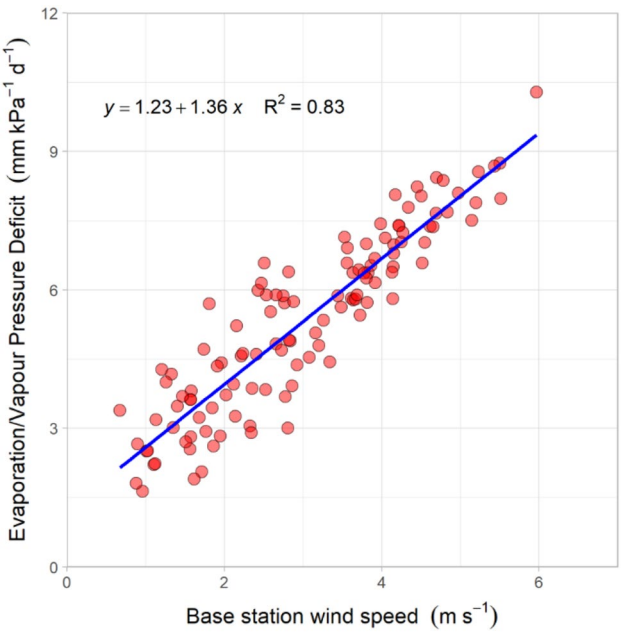

Fig. 4 Wind function relationship using high quality measurements from the first 72 days of observations

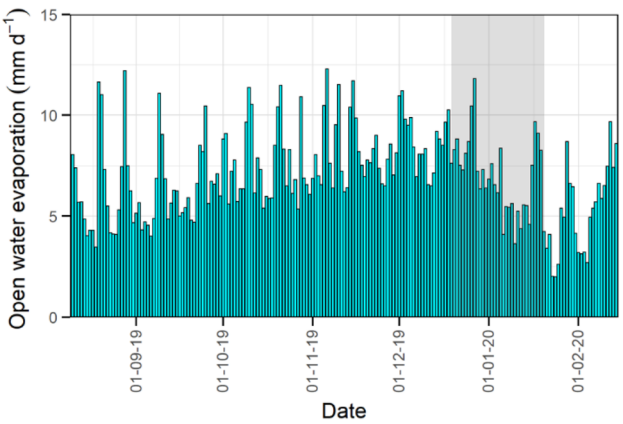

Fig. 5 Daily open water evaporation for the duration of the study period. All values are modelled using the derived wind function and land-based station meteorological data. The shaded area represents the time period where there was no open water in the TSF

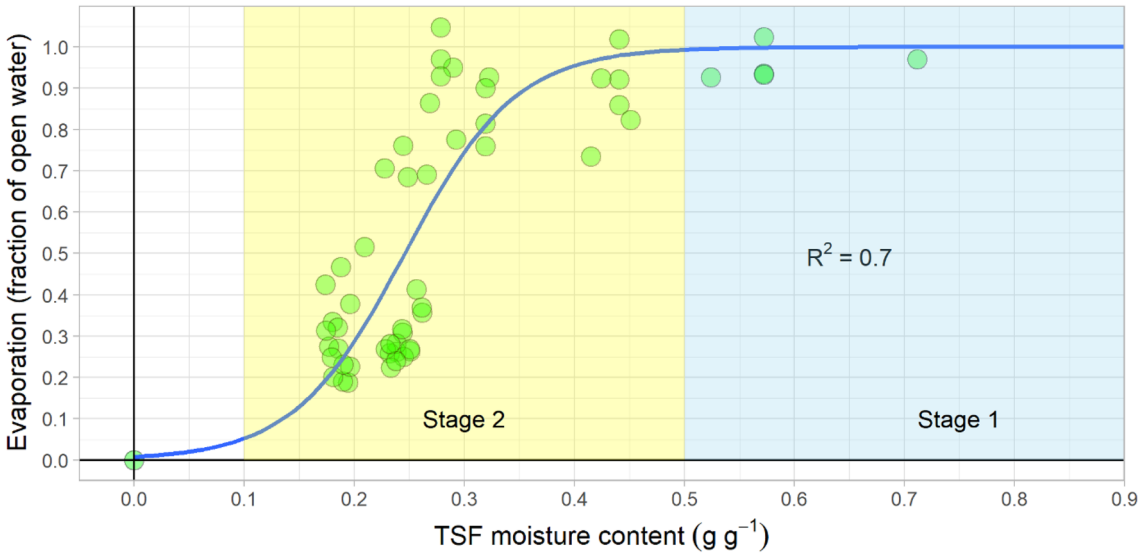

Fig. 6 Relationship between TSF gravimetric moisture content (θ) and evaporation expressed as a fraction of open water evaporation for the same day (E_{TSF}/E_O)

Tailings Beach Evaporation

During the intensive micro-lysimeter measurement period, the evaporation rate of tailings across a broad range of moisture contents was determined; this was compared to measured open water evaporation for the same day (Fig. 6), with the measured evaporation rate expressed as a fraction of open water evaporation. Tailings with a high moisture content evaporated at around the same rate as open water. This type of evaporation is referred to as Stage 1 evaporation and represents a situation where evaporation is limited only by energy availability. The tailings evaporation rate decreased markedly for tailings with a gravimetric moisture content less than 0.5 g g^{-1}. This is known as Stage 2 evaporation during which evaporation is limited by water availability (Ritchie 1972; Snyder et al. 2000).

In Fig. 6, a sigmoidal model was used to describe the relationship between TSF moisture content and evaporation. This sigmoidal model is given by Eq. (8) and represents a strong fit to the data ($R^2 = 0.71$). Using Eq. (8) with a known moisture content enables the fraction of open water evaporation to be easily derived. On any given day, the open water evaporation rate is also known (Fig. 5) and the evaporation from the tailings surface can be derived.

$$\frac{E_{TSF}}{E_O} = \frac{1}{1 + e^{-\left(\frac{\theta - 0.246}{0.0504}\right)}} \tag{8}$$

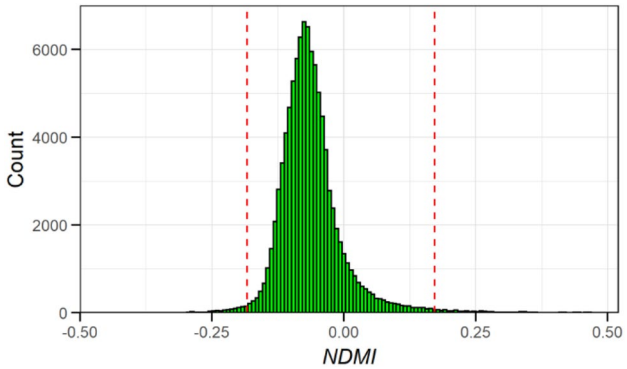

Fig. 7 Frequency distribution of *NDMI* values from the tailings beaches using Sentinel-2 scenes between 06/01/2019 and 15/02/2020. The dashed red lines show the 1st and 99th percentile of the data

TSF Evaporation

Tailings Moisture Content from Satellite

Of the 82 Sentinel-2 scenes available for the period between 6 Jan. 2019 and 15 Feb. 2020, 63 were cloud free. These cloud-free scenes were used to derive the frequency distribution of *NDMI* shown in Fig. 7. The 1st and 99th percentiles were calculated to provide the range of *NDMI* observed over time. This range was represented by a minimum *NDMI* of − 0.18 and a maximum of 0.17 and was used to scale to the range of moisture content observed across the TSF beaches.

Analysis of samples collected during the micro-lysimeter study and limited spatial sampling campaigns provided a

range of moisture content, from a minimum of 0.17 g g^{-1} for the driest areas of the tailings beach to a maximum of 0.7 g g^{-1} for tailings leaving the spigot. Records of slurry density delivered from the onsite mill show that the average moisture content of material delivered to the TSF during the study was 0.7 g g^{-1}, with a range typically between 0.65 g g^{-1} and 0.75 g g^{-1}. An average moisture content of 0.7 g g^{-1} was used as the upper limit of moisture expected across the TSF beaches, but the range of values reported by the mill was also used to look at the uncertainty in evaporation estimates. Setting the lower limit was more complicated as the lowest measured tailings moisture content, 0.17 g g^{-1}, was not necessarily the lowest likely to be observed. Analysis of spigot activation data showed that the location where the driest tailings samples were collected had not had any fresh deposition or rainfall for at least three weeks. Spigot activation times varied in response to local conditions, but fresh deposition was typically occurring every two weeks. Only 10 % of spigot reactivation times exceeded 3 weeks. Taking the measured minimum value of 0.17 g g^{-1} as being slightly above the minimum likely to be present across the TSF, the minimum value was set at 0.15 g g^{-1}. The *NDMI* was then scaled to the TSF moisture content (θ) using the linear relationship shown in Fig. 8, which is given by Eq. (9):

$$\theta = 0.434 + NDMI1.55 \tag{9}$$

Figure 8 tests the sensitivity of the relationship between *NDMI* and the tailings moisture content and its flow-through effects on predicted evaporation. Further analysis was undertaken using a range of minimum and maximum likely tailings moisture contents. An upper limit was defined using a minimum moisture content of 0.2 g g^{-1} and a maximum moisture content of 0.75 g g^{-1}, while a lower limit was defined using a minimum moisture content on 0.1 g g^{-1} and a maximum moisture content of 0.65 g g^{-1}. This range of moisture contents represents the maximum uncertainty likely in model predictions. The upper and lower limits are shown by the dashed lines in Fig. 8.

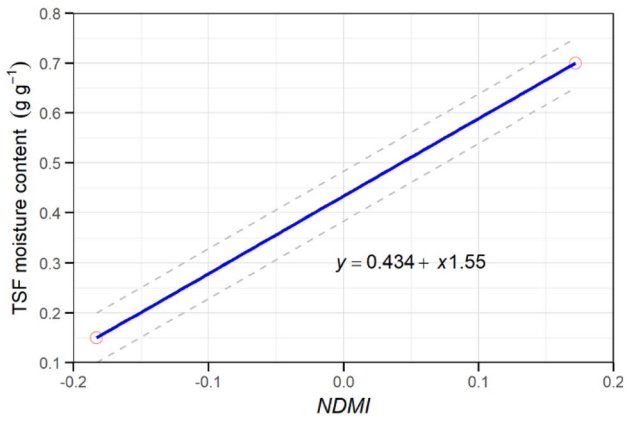

Fig. 8 Relationship between maximum and minimum *NDMI* and maximum and minimum tailings moisture content. Grey dashed lines represent the limit used for uncertainty analysis

Spatial Evaporation Prediction

For each available scene, open water was automatically assigned an evaporation fraction of 1, and the tailings beach area was assigned a surface moisture content and an evaporation fraction based on Eqs. (9) and (8), respectively. Defining the moisture content of the salt-affected area presented a challenge as this could not easily be derived from multispectral data. As an alternative, data from field sampling campaigns was used.

Two sample collection campaigns were undertaken, one on 12 Aug. 2019 and the second on 11 Oct. 2019. The spatial distribution and moisture content of samples collected from the salt-affected areas is shown in Fig. 9. During both sampling campaigns, the average moisture content for salt-affected areas was remarkably similar. On 12 Aug., the average was 0.19 g g^{-1} with a standard deviation of 0.03 g g^{-1}, while on 11 Oct., the average was 0.20 g g^{-1} with a standard deviation of 0.02 g g^{-1}. The moisture content derived during these two campaigns was used to set the moisture content at 0.2 g g^{-1} for all salt-affected areas across all scenes. The similarity in moisture content across the salt-affected areas likely reflect the drying processes that happened at the tailings surface, given the accumulation of salts, as the tailings dried beyond a certain level. The lack of spatial variability in moisture content within the salt-affected areas will introduce some uncertainty in evaporation estimation; however, it should be noted that the level of moisture shows little variation and is near the lowest experienced, hence, these areas represent the smallest fraction of open water evaporation.

Figure 10 shows the various stages of satellite image processing and TSF evaporation calculation using data from 19 Aug. 2019 as an example. Figure 10a shows the natural colour image and Fig. 10b shows the area identified as open water using the *mNDWI*. Figure 10c shows the area identified as salt affected and Fig. 10d shows the *NDMI* for the tailings beach areas. Figure 10e pulls all the surface types together to produce a spatial representation of evaporation expressed as a fraction of open water evaporation for the over-pass day and, finally, Fig. 10f shows the daily evaporation rate for all TSF pixels, which was derived using the measured open water evaporation rate for the day.

During the study period (10 Aug. 2019–15 Feb. 2020), there were a total of 38 Sentinel-2 scenes covering the TSF. The scene collection dates are shown in Fig. 11, which also indicates whether the scenes were affected by cloud cover or not. Of the 38 potential scenes, 9 were affected by cloud cover and could not be used for analysis. The biggest

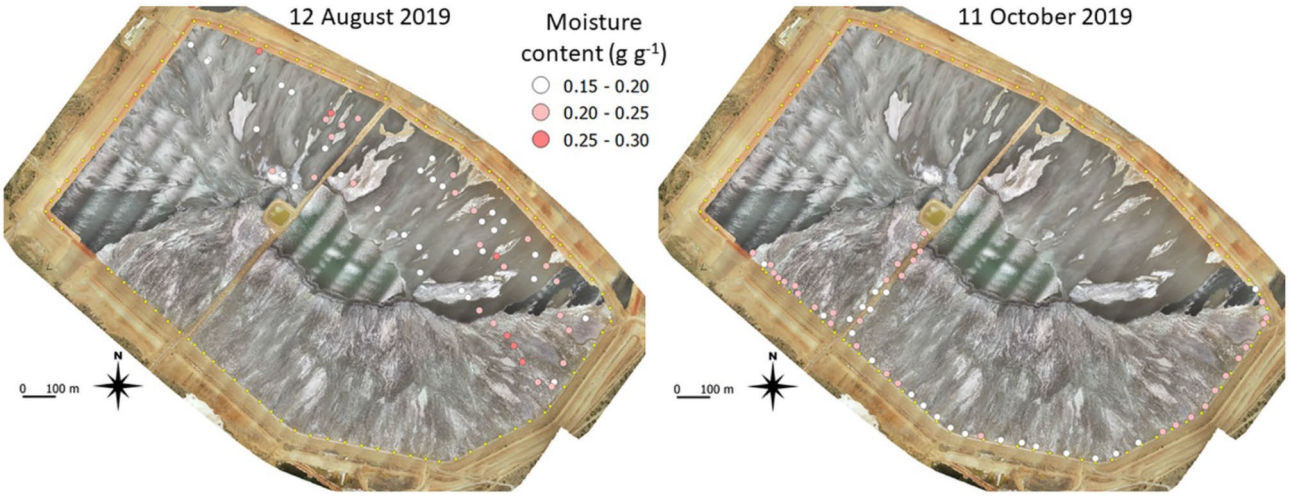

Fig. 9 Tailings grab sample locations for the salt affected areas and corresponding moisture content for sampling campaigns on 12 August 2019 and 11 October 2019

gap between cloud-free Sentinel-2 scenes during the study period was 19 days (3 consecutive scenes) during a cloudy period in early 2020.

Using days with clear Sentinel-2 scenes, it was possible to determine TSF evaporation and assess the contribution of different surface types to total evaporation. Figure 12a shows the proportion of the total TSF surface that is represented by open water on clear Sentinel-2 days. The proportion of open water area showed a decreasing trend from August 2019 through to January 2020 as conditions dried and site water supplies became scarcer, but this proportion sharply increased following rains in late January 2020. The average proportion of the surface represented by open water was 7%, the maximum was 14%, and the minimum was less than 1%. The contribution of open water to total evaporation (Fig. 12b) follows the same trend as the area of open water; however, the relative contribution to total evaporation is greater. The average proportion of total TSF evaporation contributed by open water was 11% and the maximum was 22%.

Figure 12c shows total TSF evaporation for each day with a clear Sentinel-2 scene and splits the contribution to evaporation losses from tailings beaches and open water. For these dates, total TSF evaporation averaged 5.5 ML day^{-1} with a peak value exceeding 11 ML day^{-1}. Despite there being no open water on 27 Dec. 2019, this was still the highest evaporation day for the TSF, and this was driven by particularly strong winds.

Figure 12d also shows the total TSF evaporation for each day with a clear Sentinel-2 scene but this time the results of uncertainty analysis around the relationship between *NDMI* and the tailings moisture content (Fig. 8) are also presented. The red points in this figure indicate the equivalent daily TSF evaporation when the upper bound on tailings moisture content in the relationship between *NDMI* and tailings moisture was used, while the green points provide daily TSF evaporation for analyses conducted using the lower bound in the relationship between *NDMI* and tailings moisture. Using the upper bound produced an average evaporation estimate increase of 10%; using the lower bound gave an average evaporation decrease of 15%.

Daily TSF Evaporation

The previous section outlined the process of deriving evaporation on a given satellite overpass day; however, a means by which to determine evaporation on all days was required. The approach used is demonstrated in Fig. 13, which uses example data between 12 Dec. and 15 Dec. 2019. The first and last day of this period represent satellite over pass days. Figure 13a shows the daily evaporation rate of the entire TSF surface in volumetric terms (ML day^{-1}), assuming that the entire surface was open water ($\sum E_O$). Figure 13b shows the evaporation ratio, $\sum E_{TSF} / \sum E_O$, derived on satellite overpass days with the ratio of evaporation expressed in volumetric terms. For the days between satellite overpass days, the evaporation ratio was calculated as the average of the value from the previous and next overpass day (dashed bars). Finally, Fig. 13c shows how the total TSF evaporation was calculated on all days by multiplying the evaporation ratio (Fig. 13b) by the total possible TSF evaporation for the same day (Fig. 13a).

Figure 14 shows the final daily TSF evaporation rate determined through the study period. Daily evaporation ranged from 1.9 to 11.5 ML with an average evaporation loss of 5.4 ML. The total loss of water from the TSF during

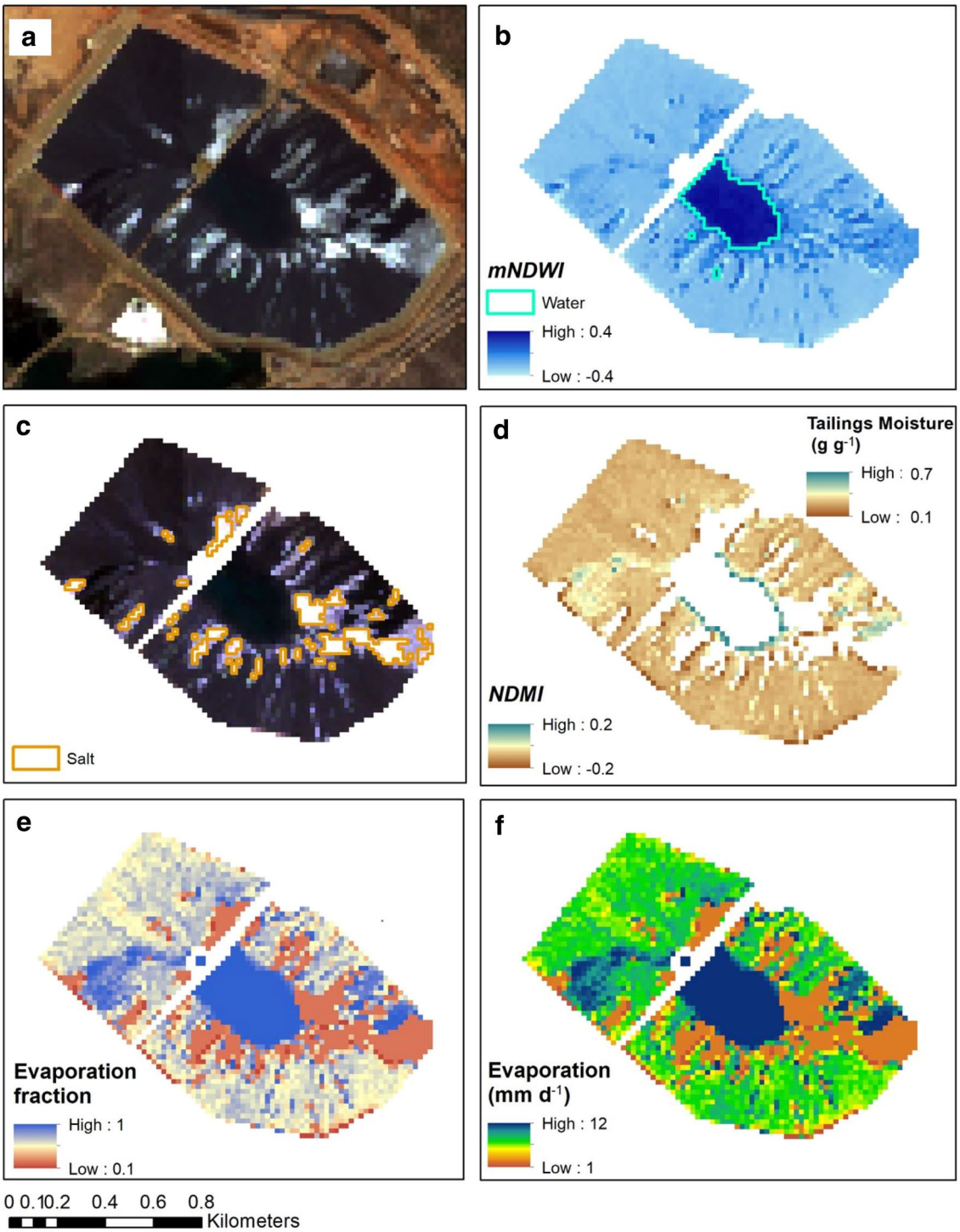

Fig. 10 Example Sentinel-2 processing from 19 August 2019 showing; **a** true colour image, **b** area identified as open water using the *mNDWI*, **c** area identified as salt affected, **d** calculated *NDMI* for and tailings moisture content for TSF beach pixels, **e** evaporation expressed as a fraction of open water evaporation for all TSF pixels and **f** evaporation (mm day^{-1}) for all pixels of the TSF on scene capture date

the 190 days of the study period was 1028 ML. On average, evaporation from the open water area of the TSF represented 10% of the total volume of water evaporated. This value ranged between 1 and 24%. mainly reflecting the extent of open water area present.

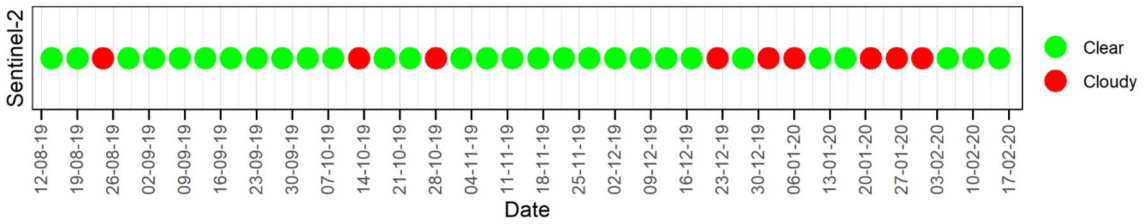

Fig. 11 Sentinel-2 overpass days showing clear scenes and scenes affected by cloud cover

Existing Water Balance Method

Figure 15 shows a comparison of the independently derived TSF evaporation rates from this study compared to those determined using the existing site water balance model. Results are compared on a monthly timestep to match the output of the water balance model. Monthly totals are similar and follow the same seasonal trends with overestimates in some months offset by underestimates in others. The total evaporation estimated for the TSF over the 157-day comparison period was 857 ML for the new approach developed in this study and 853 ML for the existing site water balance model. The total difference in evaporation between the two methods was just 4 ML or 0.4%. The results show that at monthly and longer time scales, the two approaches compare very favorably; this provides an independent validation of the proposed approach developed in this study.

Discussion

Open Water Evaporation

While floating evaporation pans have been used to determine evaporation from open water in a variety of environments (Adams et al. 1992; Gallego-Elvira et al. 2012; Masoner et al. 2008; McJannet et al. 2017, 2019; Mitsuta 1964; Rohwer 1931; Young 1947), this is the first known use in a decant pond of a TSF. The design of such pans has evolved over time as technologies improved; if rigorous data exclusion processes are adopted, high quality evaporation data can be derived. Using the temperature correction processes proposed by McJannet et al. (2017) to remove effects of temperature differences between water in the pan and the surrounding water body was important for deriving accurate results. On average, temperatures in the pan were 0.4 °C cooler that those of the surrounding water. The large store of heat in the lake water helps maintain higher temperatures relative to the pan. Failure to correct for water temperature differences would have resulted in a 5% underestimation of open water evaporation in this study.

Tailings Beach Evaporation

The micro-lysimeter measurements showed a clear transition from Stage 1 evaporation, where energy was the limiting factor, to Stage 2 evaporation, where water availability was the limiting factor, as the moisture content of the tailings decreased. This is commonly seen in evaporation studies and the shape of the relationship is typically described using piecewise (e.g. Young et al. 2007; Zeleke and Wade 2012) or sigmoidal models (e.g. Grinzato et al. 2010; Li et al. 2015), such as in this study (Eq. 8). Relating tailings moisture content to evaporation expressed as a fraction of open water evaporation for the same day normalises results and removes complications introduced by day-to-day variability in processes driving evaporation. Open water evaporation is the reference point for maximum evaporation on any given day; a similar reference evaporation rate was used by Newson and Fahey (2003).

The micro-lysimeter approach is one of the few approaches that can be used to determine evaporation from spatially discrete TSF surfaces of known moisture content; however, there are some sources of uncertainty in this method that should be acknowledged. The necessity to cap the micro-lysimeter to prevent tailings loss creates an artificial boundary to vertical water and energy movement (Evett et al. 1995), which can reduce drainage rates and reduce transport of moisture from deeper in the profile towards surface layers. Ideally, the length of a micro-lysimeter would be equal to the depth of the zero flux plane, as above this level, water losses are by evaporation alone (Verhoef and Campbell 2006). However, in a field situation with variable moisture content, the zero-flux plane is very hard to determine. Soil physical models may help in this context if detailed tailings hydraulic properties are known for the profile of interest. The effect of capping will increase with the duration of deployment; the 5-day limitation to micro-lysimeter core used in this study was implemented to minimise uncertainty. Use of micro-lysimeters beyond five days is not recommended.

An issue that this study has not dealt with directly is the influence of surface cracking on evaporation. The TSF, like many other storage facilities, regularly forms networks of

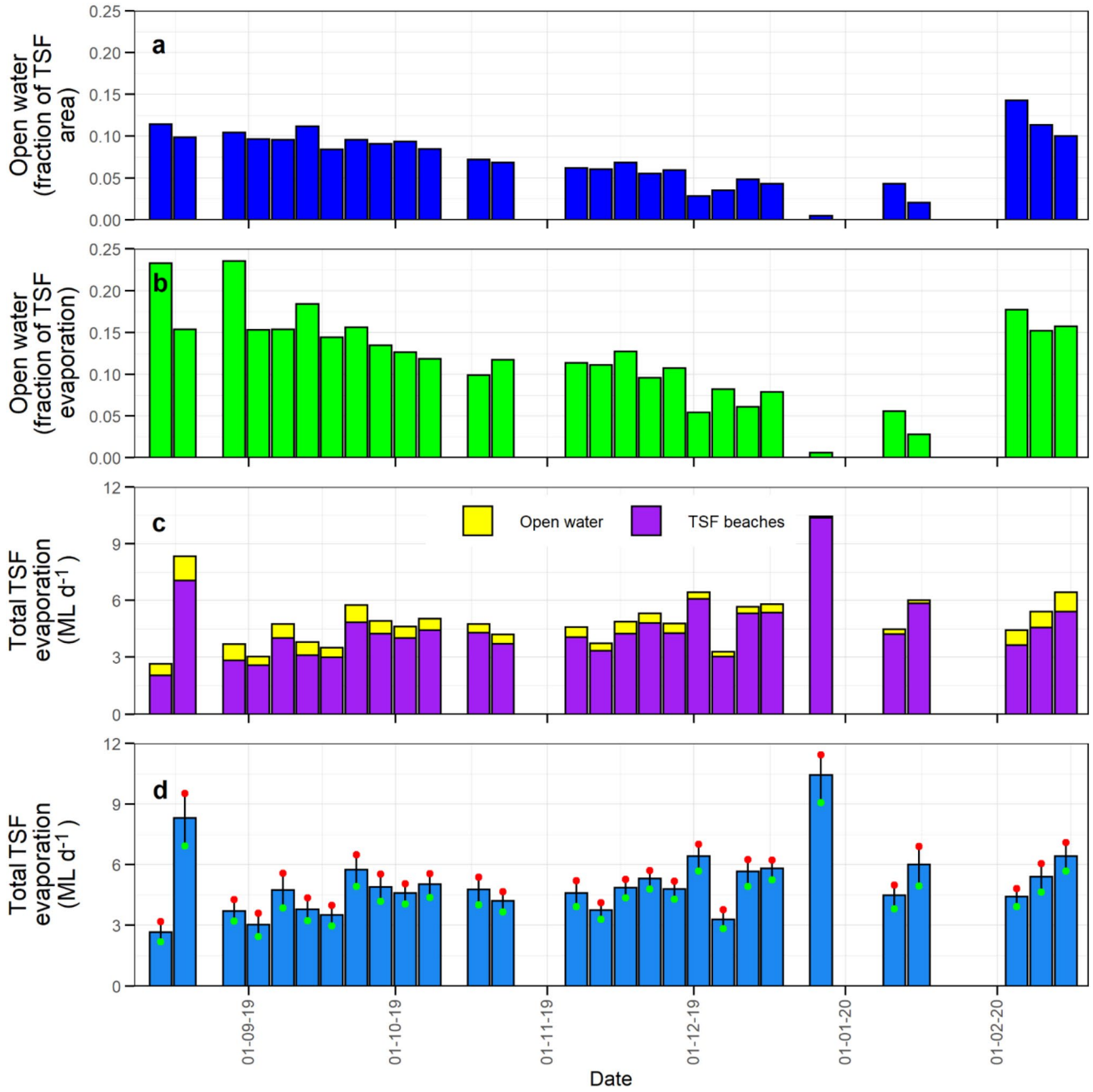

Fig. 12 **a** Open water area as a proportion of total TSF area, **b** open water evaporation as a fraction of total TSF evaporation, **c** the contributions of open water areas and tailings beach areas to total daily TSF evaporation, and **d** total daily TSF evaporation as bars with points indicating the equivalent evaporation value if the upper (red) and lower (green) bounds from the relationship between NDMI and tailings moisture (refer to Fig. 8) are used in the analysis

cracks on the surface as the tailings dry. The general consensus from the literature for soil is that cracks enhance evaporation (e.g. Newson and Fahey 2003; Poulsen et al. 2019; Ritchie and Adams 1974); however, the reported magnitude of this effect is variable and the duration over which it is maintained when a crack opens is uncertain. The effect is also potentially related to the material being investigated, e.g. the studies on gold tailings by Simms et al. (2019) and Fisseha et al. (2010), concluded that the effect of surface cracks on evaporation was minimal. The cracks could enhance evaporation as the area of tailings exposed is increased, but on the other hand, the exposed material is below the land surface and may be protected from the wind and shaded from solar radiation.

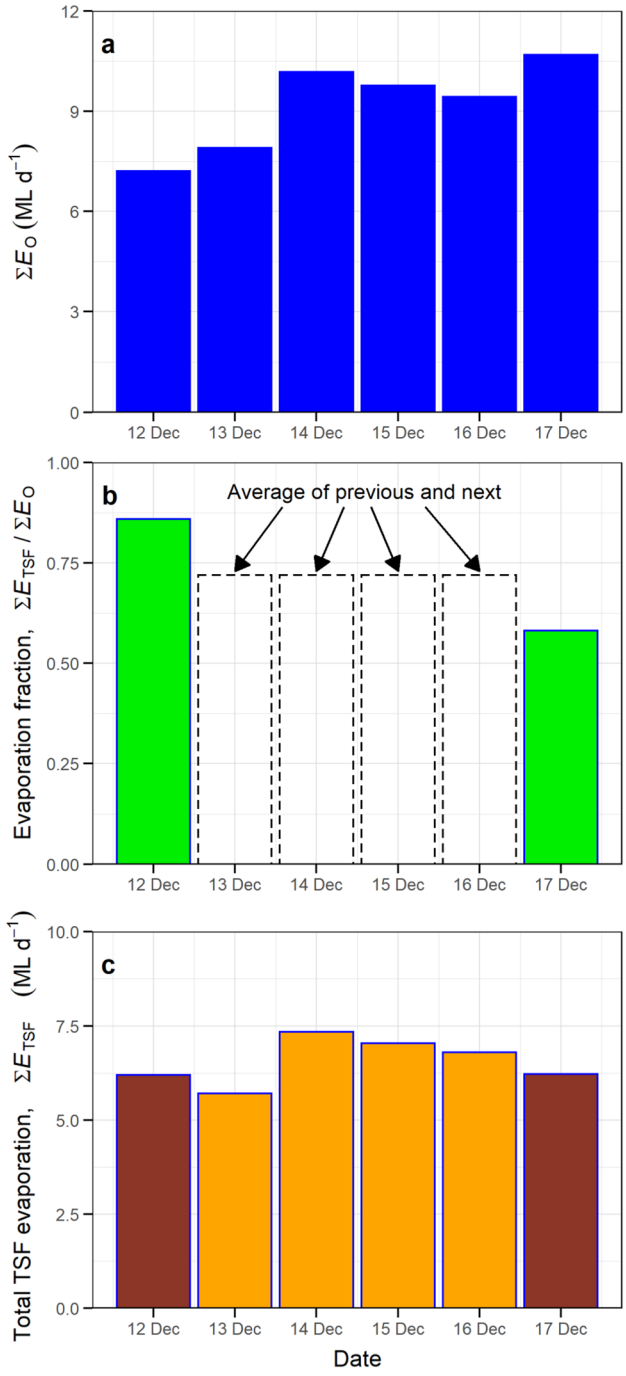

Fig. 13 Demonstration of steps used for calculating daily whole of TSF evaporation loss ($\sum E_{TSF}$) for days between Sentinel-2 satellite overpasses. **a** total TSF evaporation loss assuming the entire surface is open water ($\sum E_O$). **b** Total TSF evaporation loss as a fraction of TSF open water (i.e. $\sum E_{TSF} / \sum E_O$) for satellite overpass days (green bars). For days between satellite overpasses $\sum E_{TSF} / \sum E_O$ is estimated as the average of the same value on the previous and next satellite overpass. **c** Total TSF evaporation calculated directly on satellite overpass days (brown bars) and calculated values (orange bars) estimated using corresponding values in **a** and **b**

Fujiyasu et al. (2000) attempted to measure evaporation from cracks in drying tailings using a modified micro-lysimeter approach. Over time, the cracks were shown to increasingly contribute to total evaporation; however, this study was conducted on a TSF that was left to dry over 10 months. After 10 months, Fujiyasu et al. (2000) reported that cracks accounted for about 85% of total evaporation, but this was from a deeply desiccated system. A study by Hatano et al. (1988) in heavy clay soil found that evaporation from cracks was enhanced compared to surface soil; however, the soil was characterized by a very dry surface (0–5 cm), with moister material below.

Our qualitative field assessments suggest that the TSF material did not show a strong contrast between the moisture of the top 0–5 cm and that below, because it was not left to dry for long enough. The MRM TSF was resaturated at ≈2-week intervals and so the surface material never fully desiccated. Other authors have noted that the contribution of cracks increases as the gradient between surface and subsurface moisture increases (e.g. Adams et al. 1969; Davarzani et al. 2014). Given that the surface moisture content of the MRM TSF was rarely less than 0.2 g g^{-1}, the importance of cracks to total evaporation loss is unlikely to be as great as that observed in longer duration studies in drier environments.

The parts of the TSF most prone to cracking are the driest, and qualitative field observations suggest that these areas are also prone to salt accumulation. Other studies on tailings storages have shown that salt accumulation on the surface can reduce evaporation, so while cracks may enhance evaporation, salt crusting may reduce it. Salt may act to reduce evaporation by reflecting solar radiation, imposing a physical barrier to water transport, and decreasing the saturation vapour pressure of near-surface moisture (Newson and Fahey 2003). Saturation vapour pressure is decreased because dissolved salt ions lower the free energy of water molecules. Some of the micro-lysimeters were from salt affected areas, but none had any cracks present. While the potentially opposing effects of cracks and salt accumulation cannot be ignored completely, site characteristics suggest that the effects are likely to be minimal.

TSF Evaporation

While this is not the first study to attempt to derive tailings evaporation from satellite observations, it is the first the authors are aware of that attempts to relate on-ground measurements of evaporation processes (tailings and open water) to satellite observations. The methodology developed enabled us to explicitly account for the spatially- and temporally-varying distribution of moisture content across the tailings beaches and also track variability in the decant pond extent.

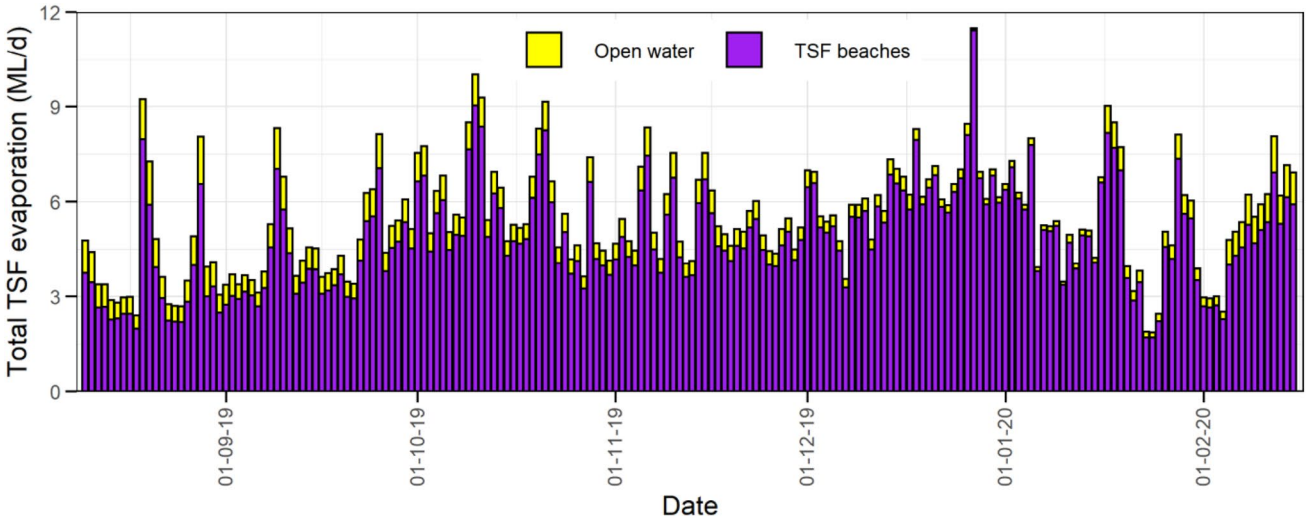

Fig. 14 Daily estimates of the volume of water evaporated from the open water area and TSF beaches across the study period

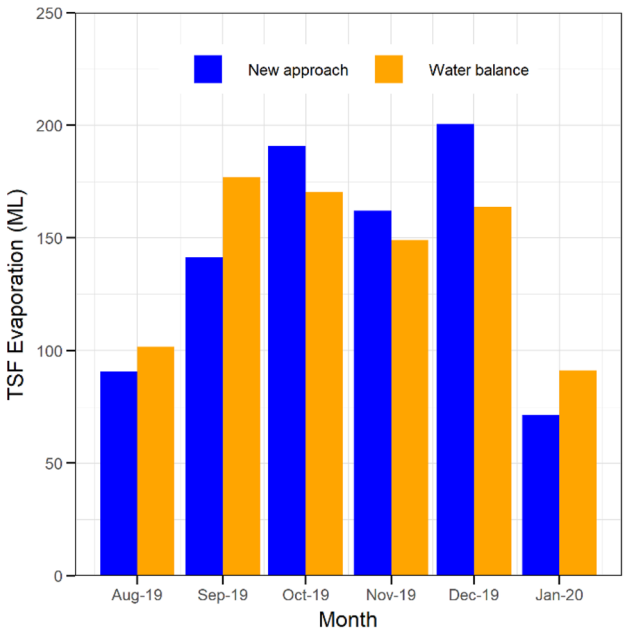

Fig. 15 Comparison of monthly estimates of evaporation volume from the MRM TSF using the site water balance model and the new approach developed in this study. Evaporation estimates cover the period between 10 August 2019 and 13 January 2020. NB. August 2019 and January 202 are not complete months

Entezari et al. (2016) related hyperspectral observations to water content in the laboratory with the aim of applying the technique to satellite observations. They also developed an approach to determine evaporation using a similar method as this current study, except they used a modelled representation of potential evaporation rather than actual open water evaporation. In another study, Keller et al. (2018) used Landsat imagery to derive spatially distributed evaporation estimates on a monthly basis using potential evaporation determined using weather station data. Other studies have used remote sensing to determine spatial distribution of tailings moisture content but have not included attempts to determine evaporation. For example, Chetty (2013) used WorldView-2 imagery from two dates to define relative wetness across a TSF surface and Zwissler et al. (2017) used thermal remote sensing with a drone to define a relationship between temperature and tailings moisture content.

A key step in relating satellite observations to evaporation rates was specifying the relationship between *NDMI* and tailings moisture content. As safety protocols prohibited widespread sampling across the TSF, a linear fit between maximum and minimum observed moisture contents was used. Analysis was undertaken to investigate the sensitivity of results to uncertainties in maximum and minimum moisture contents. The minimum moisture content ranged between 0.1 and 0.2 g g^{-1}; this should be regarded as the largest possible range. Several tailings samples with moisture content less than 0.2 g g^{-1} were collected on site so this value is already known to be unrealistically high. The lower limit of 0.1 g g^{-1} is also likely to be at the lower end for tailings material of this texture. Tailings from the MRM TSF have a particle size distribution where nearly 80 % of the material is clay and silt (i.e. < 0.075 mm). Such a material has a high residual water holding capacity and water molecules are tightly bound in the tailings matrix. While such low values may be feasible for the tailings material, they would only occur after extended exposure to drying conditions, and this in unlikely to occur given the typical two week reactivation period for spigots at this site. The upper limit of moisture content is more certain as the records of slurry density delivered from the MRM mill show that average moisture content of material delivered to the TSF during

the study was 0.7 g g^{-1}. This did vary slightly over time but was typically between 0.65 and 0.75 g g^{-1}. Using the upper uncertainty bound resulted in an average evaporation estimate increase of 10%. Using the lower uncertainty bound resulted in an average evaporation decrease of 15%. Given this uncertainty analysis extended to bounds beyond what could be reasonably expected under field conditions, evaporation estimation uncertainty is likely to be less than 10%.

The approach used to relate *NDMI* to moisture content across the TSF utilised a linear relationship despite only having values at the dry and wet end of the range of potential moisture content values. There is the possibility that a non-linear relationship may exist; however, results from other studies suggest that this is unlikely to be the case. In laboratory experiments, Gao (1996) clearly showed that the *NDMI* was linearly related to water availability in the absence of vegetation, and noted that the *NDMI* uses the *NIR* spectrum to detect variations in leaf structure and leaf dry matter and the *SWIR* to detect variations in vegetation and moisture content. In the case of the TSF, changes to the *NDMI* will be most sensitive to SWIR variation. The importance of *SWIR* for detecting changes in moisture content has also been noted by Ceccato et al. (2002). Further evidence to support the use of a linear fit comes from a number of separate fields studies in areas with little or no vegetative cover (e.g. Jovanovic et al. 2014; Tarik et al. 2019; Wang et al. 2008).

Gaps in Sentinel-2 scenes, particularly those associated with cloudy conditions, add uncertainty to TSF evaporation estimates. Cloud affected periods associated with saturating rainfall (e.g. > 20 mm) are likely to introduce the greatest uncertainty in evaporation estimates as the TSF surface condition will have changed to relatively uniform wetness without being captured by satellite observations. Evaporation estimates during inter-scene periods that experience saturating rainfall are likely to represent underestimates of evaporation; however, evaporation on days that experience heavy rainfall is typically low. During this study, there were only six days where total rainfall exceeded 20 mm; if it is assumed that the evaporation fraction on these days was 1 rather than the value derived from the average of the previous and next overpass day, then evaporation on these days was underestimated by 15 % on average (range = 12–16 %). Over the study, this equates to 5.0 ML, which is less than 0.5 % of the estimated total evaporation. Expanding this analysis to include days where rainfall exceeded 10 mm (13 in total) equates to a 9.0 ML or 1 % underestimation of evaporation across the study period. Hence, while such gaps introduce uncertainty, the effect is unlikely to be large.

The approach developed in this study can be automated to provide ongoing TSF evaporation estimates using the land-based monitoring station data and automated processing of Sentinel-2 scenes. Compared to the traditional site water balance method, the approach detailed here can be applied in a timelier manner. In future studies, it may be possible to draw on multispectral scenes from other satellite missions (e.g. Landsat) to fill gaps and produce a more complete temporal satellite coverage for the TSF. Such an approach would require fusion of products with different temporal and spatial resolution and development of techniques for accommodating the differences that exist in spectral bands between products.

Conclusions

Evaporation from TSFs is particularly hard to quantify as the degree of surface wetness varies spatially and temporally, and local moisture content typically depends on the time since tailings deposition and the prevailing climate. This study addressed these issues at active TSF at McArthur River Mine by using a combination of field measurements and satellite observations. The field measurements yielded a relationship between evaporation rate and surface moisture content while the satellite analysis provided the temporal and spatial variability in surface moisture content. High quality evaporation measurements were used to build a robust evaporation model, which enabled determination of daily evaporation rates for the entire 190-day study period. Open water evaporation rates were crucial for determination of TSF evaporation as they provided the maximum evaporation rate, or reference rate, against which evaporation from the tailings beaches was scaled.

Micro-lysimeter measurements of evaporation from the TSF beaches showed a strong relationship between moisture content and evaporation expressed as a fraction of open water evaporation. The spatial and temporal variation in TSF moisture content was determined using Sentinel-2 *NDMI*, which was scaled to actual tailings moisture content using on-ground observations. Sensitivity analysis suggested that uncertainty in evaporation estimates was likely less than ± 10%. Comparison of total TSF evaporation using the approach developed in this study against the existing site water balance model showed very good agreement in results with a difference in cumulative evaporation of just 4 ML or 0.4% over a period of 157 days. While TSFs present a unique challenge for evaporation estimation, the methodology used in this study, which combined measurements, models, and satellite observations, lends itself to application at TSFs around the world.

Acknowledgements The authors thank Danielle Darcy, Emerson Pollard, Garry Law and Benjamin Musitano for helping with field data collection. We also thank numerous other McArthur River Mine staff who provided data and assistance where required. Sentinel-2 data was provided by the European Space Agency. Drone imagery was supplied

by the MRM surveying department. This study was co-funded by Glencore, McArthur River Mine, and CSIRO.

References

Adams J, Leibfried R, Spoden G, Alderdice L (1992) Surface water evaporation from mine pits in Minnesota. In: Proceedings of National Meeting of the American Society for surface mining and reclamation, pp 268–279

Adams JE, Ritchie JT, Burnett E, Fryrear D (1969) Evaporation from a simulated soil shrinkage crack. Soil Sci Soc Am J 33:609–613. https://doi.org/10.2136/sssaj1969.03615995003300040034x

Adiansyah JS, Rosano M, Vink S, Keir G (2015) A framework for a sustainable approach to mine tailings management: disposal strategies. J Clean Prod 108:1050–1062. https://doi.org/10.1016/j.jclepro.2015.07.139

Boast C (1986) Evaporation from bare soil measured with high spatial resolution. Methods of soil analysis: part 1—physical and mineralogical methods: agronomy monograph no 9. Soil Science Society of America, Washington, pp 889–900. https://doi.org/10.2136/sssabookser5.1.2ed.c35

Boast CW, Robertson TM (1982) A "micro-lysimeter" method for determining evaporation from bare soil: description and laboratory evaluation. Soil Sci Soc Am J 46:689–696. https://doi.org/10.2136/sssabookser5.1.2ed.c35

Ceccato P, Flasse S, Grégoire J-M (2002) Designing a spectral index to estimate vegetation water content from remote sensing data: Part 2. Validation and applications. Remote Sens Environ 82:198–207. https://doi.org/10.1016/S0034-4257(02)00036-6

Chetty P (2013) Monitoring of mine tailings using satellite and lidar data. In: Proceedings of SASGI Ekurhuleni, South Africa, pp 1–15

Daamen CC, Simmonds LP, Wallace JS, Laryea KB, Sivakumar MVK (1993) Use of microlysimeters to measure evaporation from sandy soils. Agric For Meteorol 65:159–173. https://doi.org/10.1016/0168-1923(93)90002-Y

Dalton J (1802) Experimental essays on the constitution of mixed gases; on the force of steam or vapour from water and other liquids at different temperatures, both in a Torricellian vacuum and in air; on evaporation; and on the expansion of gases by heat. Lit Philos Soc Manch Mem 5–11:535–602

Davarzani H, Smits K, Tolene RM, Illangasekare T (2014) Study of the effect of wind speed on evaporation from soil through integrated modeling of the atmospheric boundary layer and shallow subsurface. Water Resour Res 50:661–680. https://doi.org/10.1002/2013WR013952

Edraki M, Baumgartl T, Manlapig E, Bradshaw D, Franks DM, Moran CJ (2014) Designing mine tailings for better environmental, social and economic outcomes: a review of alternative approaches. J Clean Prod 84:411–420. https://doi.org/10.1016/j.jclepro.2014.04.079

Entezari I, Rivard B, Lipsett MG, Wilson GW (2016) Prediction of water content and normalized evaporation from oil sands soft tailings surface using hyperspectral observations. Can Geotech J 53:1742–1750. https://doi.org/10.1139/cgj-2015-0416

Evett SR, Warrick AW, Matthias AD (1995) Wall and capping effects on microlysimeter temperatures and evaporation. Soil Sci Soc Am J 59:329–336. https://doi.org/10.2136/sssaj1995.03615995005900020009x

Fisseha B, Bryan R, Simms P (2010) Evaporation, unsaturated flow, and salt accumulation in multilayer deposits of "paste" gold tailings. J Geotech Geoenviron Eng 136:1703–1712. https://doi.org/10.1061/(ASCE)GT.1943-5606.0000367

Fujiyasu Y, Fahey M, Newson T (2000) Field investigation of evaporation from freshwater tailings. J Geotech Geoenviron Eng 126:556–567. https://doi.org/10.1061/(ASCE)1090-0241(2000)126:6(556)

Gallego-Elvira B, Baille A, Martin-Gorriz B, Maestre-Valero J, Martinez-Alvarez V (2012) Evaluation of evaporation estimation methods for a covered reservoir in a semi-arid climate (southeastern Spain). J Hydrol 458:59–67. https://doi.org/10.1016/j.jhydrol.2012.06.035

Gao B-C (1996) NDWI—a normalized difference water index for remote sensing of vegetation liquid water from space. Remote Sens Environ 58:257–266. https://doi.org/10.1016/S0034-4257(96)00067-3

Grinzato E, Cadelano G, Bison P (2010) Moisture map by IR thermography. J Mod Opt 57:1770–1778. https://doi.org/10.1080/09500341003731597

Hatano R, Nakamoto H, Sakuma T, Okajima H (1988) Evapotranspiration in cracked clay field soil. Soil Sci Plant Nutr 34:547–555. https://doi.org/10.1080/00380768.1988.10416470

Jones H, Boger DV (2012) Sustainability and waste management in the resource industries. Ind Eng Chem Res 51:10057–10065. https://doi.org/10.1021/ie202963z

Jovanovic N, Garcia CL, Bugan RD, Teich I, Rodriguez CMG (2014) Validation of remotely-sensed evapotranspiration and NDWI using ground measurements at Riverlands, South Africa. Water SA 40:211–220

Keller J, Hendrickx J, Milczarek M, Partey F, Geddis M (2018) High resolution estimates of tailings facility evaporation using landsat data. In: Paper presented at the risk to opportunity, 11th ICARD IMWA, MWD conference, pp 1105–1110

Leavy J (2018) Yangibana project western Australia. Feasibility study design. Tailings storage facilities design report. Appendix 6–3. Williams ATC2021. http://www.epa.wa.gov.au/sites/default/files/PER_documentation2/Appendix%206-3%20Tailings%20Storage%20Facilities%20Design%20Report%20Part%201.pdf. Accessed 16 Apr 2021

Li Y, Zhou J, Wang H, Li D, Jin R, Zhou Y, Zhou Q (2015) Integrating soil moisture retrieved from L-band microwave radiation into an energy balance model to improve evapotranspiration estimation on the irrigated oases of arid regions in northwest China. Agric For Meteorol 214–215:306–318. https://doi.org/10.1016/j.agrformet.2015.08.260

Mallick J, Singh CK, Shashtri S, Rahman A, Mukherjee S (2012) Land surface emissivity retrieval based on moisture index from LANDSAT TM satellite data over heterogeneous surfaces of Delhi city. Int J Appl Earth Observ Geoinf 19:348–358. https://doi.org/10.1016/j.jag.2012.06.002

Masoner JR, Stannard DI, Christenson SC (2008) Differences in evaporation between a floating pan and class A pan on land. J Am Water Resour Assoc 44:552–561. https://doi.org/10.1111/j.1752-1688.2008.00181.x

McJannet D, Hawdon A, Baker B, Ahwang K, Gallant J, Henderson S, Hocking A (2019) Evaporation from coal mine pit lakes: measurements and modelling. In: Paper presented at the proceedings of the 13th international conference on mine closure, Perth, pp 1391–1404. https://doi.org/10.36487/ACG_rep/1915_109_McJannet

McJannet D, Vertessy R, Clifton C (2000) Observations of evapotranspiration in a break of slope plantation susceptible to periodic drought stress. Tree Physiol 20:169–177. https://doi.org/10.1093/treephys/20.3.169

McJannet D, Hawdon A, Van Niel T, Boadle D, Baker B, Trefry M, Rea I (2017) Measurements of evaporation from a mine void lake and testing of modelling approaches. J Hydrol 555:631–647. https://doi.org/10.1016/j.jhydrol.2017.10.064

Mitsuta Y (1964) A new floating evaporimeter. Spec Contrib Geophys Inst Kyoto Univ 12:119–125

MRM (2017) McArthur river mine overburden management project—Environmental Impact Statement (EIS), Ch 8: water resources. MRM, New York

Newson TA, Fahey M (2003) Measurement of evaporation from saline tailings storages. Eng Geol 70:217–233. https://doi.org/10.1016/S0013-7952(03)00091-7

Poulsen TG, Cai W, Garg A (2019) Water evaporation from cracked soil under moist conditions as related to crack properties and near-surface wind speed. Eur J Soil Sci 2020:1–14. https://doi.org/10.1111/ejss.12926

Ritchie JT (1972) Model for predicting evaporation from a row crop with incomplete cover. Wat Resour Res 8:1204–1213. https://doi.org/10.1029/WR008i005p01204

Ritchie J, Adams J (1974) Field measurement of evaporation from soil shrinkage cracks. Soil Sci Soc Am J 38:131–134. https://doi.org/10.2136/sssaj1974.03615995003800010040x

Rohwer C (1931) Evaporation from free water surfaces: technical bulletin no. 271. US Department of Agriculture, Washington

Rykaart EM, Wilson GW, Fredlund D, Currey N (2001) A spatial flux boundary model for tailings dams. In: Proceedings of 54th Canadian geotechnical conference, Calgary, Alberta, Canada, pp 17–19

Schoenberger E (2016) Environmentally sustainable mining: the case of tailings storage facilities. Resour Policy 49:119–128. https://doi.org/10.1016/j.resourpol.2016.04.009

Simms P, Grabinsky M, Zhan G (2007) Modelling evaporation of paste tailings from the Bulyanhulu mine. Can Geotech J 44:1417–1432. https://doi.org/10.1139/T07-067

Simms P, Soleimani S, Mizani S, Daliri F, Dunmola A, Rozina E, Innocent-Bernard T (2019) Cracking, salinity and evaporation in mesoscale experiments on three types of tailings. Environ Geotech 6:3–17. https://doi.org/10.1680/jenge.16.00026

Šimůnek J, van Genuchten MT, Šejna M (2008) Development and applications of the HYDRUS and STANMOD software packages and related codes. Vadose Zone J 7:587–600. https://doi.org/10.2136/vzj2007.0077

Snyder R, Bali K, Ventura F, Gomez-MacPherson H (2000) Estimating evaporation from bare or nearly bare soil. J Irrig Drain Eng 126:399–403. https://doi.org/10.1061/(ASCE)0733-9437(2000)126:6(399)

Solgi N (2017) Water balance of metal mining tailings management facilities: influence of climate conditions and tailings management options. PhD Thesis, University of British Columbia

Tarik B, Hayat L, Rachid H, Riad B, Abdelghani B, Bernard T (2019) Support irrigation water management of cereals using optical remote sensing and modeling in a semi-arid region. In: Moha E-A, El Loubna M (eds) Geospatial technologies for effective land governance. Global IGI, Hershey, pp 124–145. https://doi.org/10.4018/978-1-5225-5939-9.ch008

Verhoef A, Campbell CL (2006) Evaporation measurement. Encycl Hydrol Sci. https://doi.org/10.1002/0470848944.hsa043

Wang L, Qu JJ, Hao X, Zhu Q (2008) Sensitivity studies of the moisture effects on MODIS SWIR reflectance and vegetation water indices. Int J Remote Sens 29:7065–7075. https://doi.org/10.1080/01431160802226034

Weilenmann A (1877) Die verdunstungdes Wassers, Schweiz Met Beob12:268–368

Wilson EH, Sader SA (2002) Detection of forest harvest type using multiple dates of Landsat TM imagery. Remote Sens Environ 80:385–396. https://doi.org/10.1016/S0034-4257(01)00318-2

Xu H (2006) Modification of normalised difference water index (NDWI) to enhance open water features in remotely sensed imagery. Int J Remote Sens 27:3025–3033. https://doi.org/10.1080/01431160600589179

Xu C, Qu JJ, Hao X, Wu D (2020) Monitoring Surface soil moisture content over the vegetated area by integrating optical and SAR Satellite observations in the permafrost region of Tibetan Plateau. Remote Sens 12:183. https://doi.org/10.3390/rs12010183

Young AA (1947) Some recent evaporation investigations. Eos Trans AGU 28:279–284. https://doi.org/10.1029/TR028i002p00279

Young C et al (2007) Modeling shallow water table evaporation in irrigated regions. Irr Drain Sys 21:119–132. https://doi.org/10.1007/s10795-007-9024-4

Zeleke KT, Wade LJ (2012) Evapotranspiration estimation using soil water balance, weather and crop data. In: Ihrmak A (ed) Evapotranspiration-remote sensing and modeling. IntechOpen, London, pp 41–58. https://doi.org/10.5772/17489

Zwissler B, Oommen T, Vitton S, Seagren EA (2017) Thermal remote sensing for moisture content monitoring of mine tailings: laboratory study. Environ Eng Geosci 23:299–312. https://doi.org/10.2113/gseegeosci.23.4.299